One-Pot Ultrafast Self-Assembly of Autofluorescent Polyphenol-Based Core@Shell Nanostructures and Their Selective Antibacterial Applications

Jinbo Fei,[†] Jie Zhao,[†] Cuiling Du,[‡] Anhe Wang,[‡] He Zhang,[†] Luru Dai,[‡] and Junbai Li[†,‡,*]

[†]Beijing National Laboratory for Molecular Sciences, CAS Key Lab of Colloid, Interface and Chemical Thermodynamics, Institute of Chemistry, Chinese Academy of Sciences, Zhong Guan Cun, Beijing 100190, China and [‡]National Center for Nanoscience and Technology, Beijing 100190, China

ABSTRACT We demonstrate that large-scale autofluorescent tea polyphenol (TP)-based core@shell nanostructures can be assembled by one-pot preparation under microwave irradiation within 1 min. The formation mechanism of the heterogeneous well-defined core@shell nanocomposites involves microwave-assisted oxidation-inducing self-assembly and directed aggregation. The strategy is general to construct Ag@TP and Au@TP nanocomposites. Moreover, a simple galvanic replacement reaction was introduced to synthesize hollow Au/Ag@TP bioconjugates with near-infrared (NIR) absorption, which could be exploited for NIR cancer diagnosis and treatment. It could be expected that more complex alloy@TP nanostructures can be obtained under proper reaction conditions. Furthermore, as a first application, it is shown that the heterogeneous Ag@TP nanostructures can strongly inhibit *Escherichia coli* growth, while they exhibit no obvious normal cell toxicity. The sharp contrast of the two effects promises that the nanocomposites are excellent low toxicity biomaterials for selective antibacterial treatment.

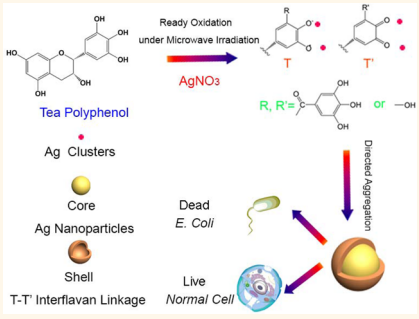

KEYWORDS: core–shell nanostructure · polyphenol · autofluorescence · selective antibacterial materials · microwave chemistry

Co-assembly of two or more components with well-defined nanostructures can introduce advanced chemical, physical, and biological properties.[1−4] However, most reported approaches include many lengthy operation procedures. Up to now, it is still a great challenge to design and develop innovative single-pot methods to assemble core@shell nanostructures with novel functions.[5,6]

Green chemistry provides an environmentally friendly strategy to fabricate functional nanostructures.[7−9] Recently, it has been a very hot topic using natural biomass as reactants or directional building blocks for constructing bionanomaterials.[10−13] As one kind of typical biomass, tea polyphenols (TP) are a group of polyphenol compounds extracted from tea leaves or coffee and collectively referred to as catechins. As a long-time popular drink, their physicochemical properties have been well-investigated and new biofunctions such as antioxidant, antiradical, antibacterial activities, and treatment of Alzheimer's disease have been reported.[14−17] Very recently, Li *et al.* reported that porous and hollow TP spheres were fabricated by Cu^{2+}-mediated oxidative coupling assembly.[18] These TP-based spheres were redox- and alkali-responsive and possessed a great potential application as intracellular drug carriers. Also, there have been several excellent reports which used TP for the reduction of Ag^{+} and $AuCl_4^{-}$ to prepare Ag and Au nanoparticles.[19−23] For instance, as a pioneering study, Varma and co-workers introduced a green approach to prepare Ag and Pd nanocrystals employing coffee and tea extract at room temperature.[19] Further study will be very helpful to explore new ways for assembling versatile TP-based complex nanostructures for biomedical applications.

Herein, by the strategy of molecular self-assembly, we introduce a simple and ultrafast method to construct autofluorescent metal@TP nanostructures, as shown in Figure 1. In a typical experiment, TPs were extracted from broadleaf holly leaves by using boiled water at 95 °C. Then, after

* Address correspondence to jbli@iccas.ac.cn.

Received for review June 10, 2014 and accepted August 8, 2014.

Published online August 08, 2014
10.1021/nn504077c

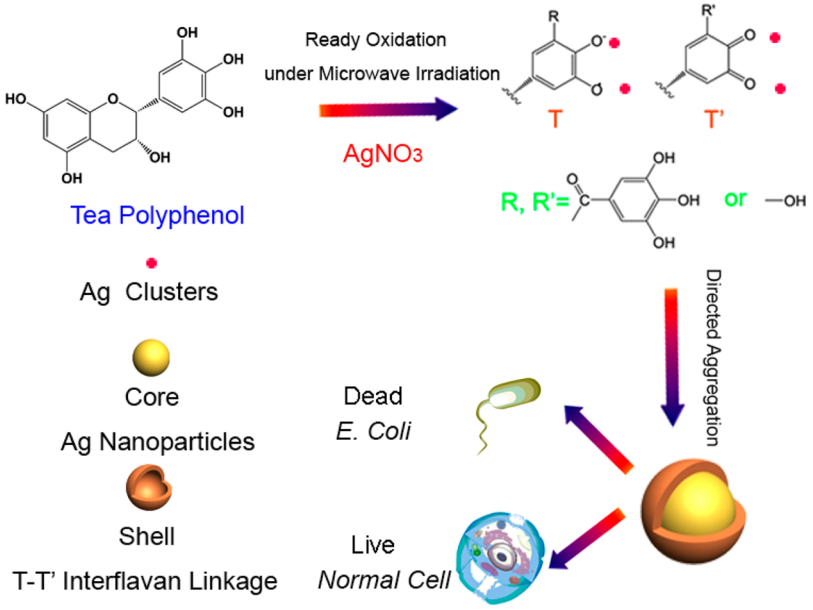

Figure 1. Schematic illustration of self-assembly of polyphenol-based core@shell nanostructures within 1 min using microwave-assisted green chemistry. Thereinto, Ag@TP uses selective inhibition for bacteria growth and nontoxicity to normal cells.

being cooled to room temperature, a solution containing noble metal ions was added into the extract mentioned above. Under microwave irradiation, through ready oxidation-inducing self-assembly and following directed aggregation, large-scale well-defined metal@TP nanostructures could be obtained. The strategy using microwave-assisted green chemistry will pave a new and general route to synthesize other TP-based core@shell nanostructures with various biofunctions.

RESULTS AND DISCUSSION

Take the $AgNO_3$—TP reaction system as the first example. The photo image of the product (the inset in Figure 2A) reveals that the relevant reaction designed was rational because the yellow-red color represents the formation of typical Ag colloids. Figure 2A shows that the product was nanoparticles with a clear boundary at large scale. In addition, SEM image in Figure 2A with higher magnification shows that a single nanoparticle with a diameter of about 80 nm was of irregular morphology. As shown in Figure 2B, the result of TEM measurement indicates that the mean diameter of the nanoparticles is about 78 nm (obtained from the statistical result of more than 30 nanoparticles by ImageJ), consistent with that of SEM. Also, some of nanoparticles were entangled with each other. In particular, the TEM image with higher magnification shows that the a single heterogeneous core@shell nanostructured nanoparticle comprised two components with distinct electronic densities. The diameter of the core is about 60 nm, and the thickness of the shell is about 8 nm.

To investigate the precise constitution of the heterogeneous nanostructures, electronic dispersive spectroscopy (EDS) (Supporting Information Figure S1A) was first employed to demonstrate that the nanocomposites contain three main chemical components (Ag, C, and O). Moreover, the corresponding element linear mapping of a single nanoparticle (Figure 3A,B) clearly shows the distribution of the elements of Ag (black), C (red), and O (blue). It can be rationally deduced that the hybrid nanoparticle is composed of Ag as the core and TP as the shell. Furthermore, X-ray diffraction (XRD) was employed to examine the phase of the product. As shown in Figure 3C, the peaks of the product can be attributed to the bulk cubic Ag patterns. The diffraction features appear at about 38.1, 44.1, and 64.4°, corresponding to the (111), (200), and (220) planes of the cubic phase of Ag, respectively. It can be deduced from the pattern that the lattice constant is 0.4091 nm, which is very close to the reported data (JCPDS No. 04-0783).[19] Moreover, as presented in Figure 3D, the core@shell nanostructure suspension exhibits an absorption band at about 456 nm, which is a typical plasmon resonance peak of spherical Ag nanoparticles. In addition, another peak appears at about 280 nm, which is similar to the maximum absorption of TP after oxidation.[18]

Furthermore, Fourier transform infrared spectroscopy (FTIR) and X-ray photoelectronic spectroscopy (XPS) were used to examine the changes of chemical structures before and after assembly. The relevant FTIR patterns in Figure S2 reveal that, after the oxidation by Ag^+, TP absorption centered at 3413 cm^{-1} is broadened, an absorption at 2935 cm^{-1} is varied remarkably, and TP C═O absorption is shifted from 1723 to 1706 cm^{-1}. Furthermore, the decreased intensity and broadening of absorptions in the range of 400—800 cm^{-1} show the changes of the aromatic ring

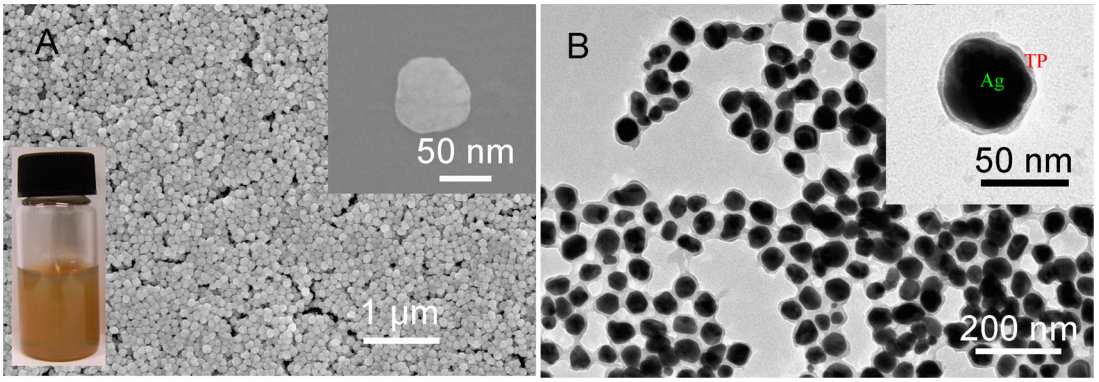

Figure 2. (A) SEM images of Ag@TP with lower and higher magnification. The inset is its optical image. (B) TEM images of the products with lower and higher magnification.

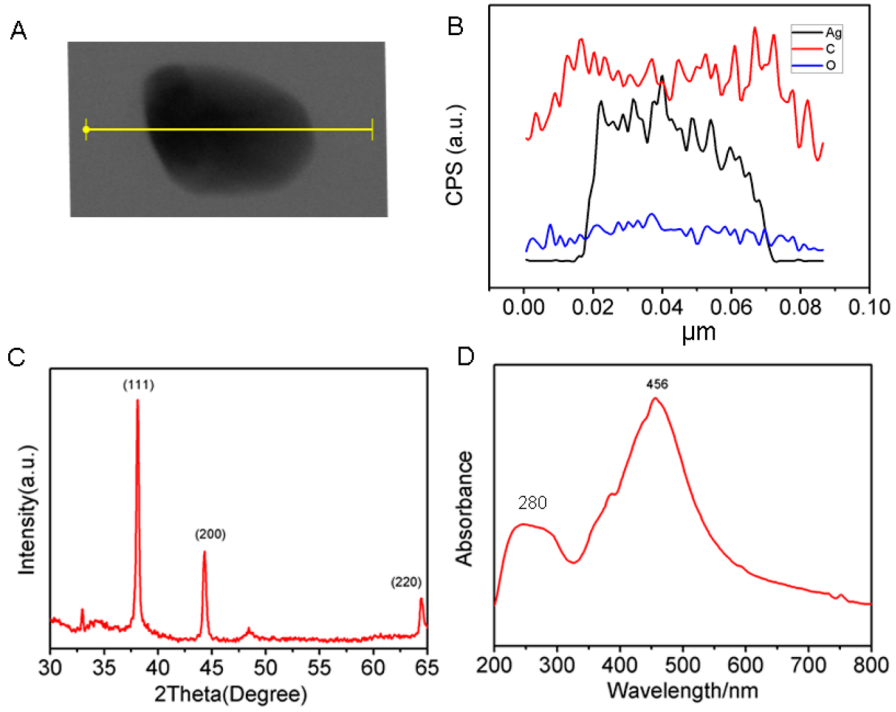

Figure 3. (A) STEM image of a single Ag@TP nanoparticle; (B) relevant element linear mapping: Ag, C, and O. (C) XRD pattern of the Ag@TP nanocomposites and (D) UV−vis spectrum of their dispersed suspensions.

moieties. The absorption at 1510 cm^{-1} could be ascribed to C−C aromatic rings, and the absorption at 1124 cm^{-1} could be attributed to the symmetric vibrations of the ether bond in core@shell nanoparticles. The results indicate that TPs were oxidized by $AgNO_3$, in good agreement with those in the previous report.[18] In addition, the corresponding XPS pattern shown in Figure S3A reveals that the main elements of tea extract are C and O. The small quantity of nitrogen could account for some types of proteins from tea extract. Figure S3B shows that, after reaction, the existence of a very small quantity of Ag indicates that Ag nanoparticles as the core exist in the heterogeneous nanostructures because XPS only detects the sample with limited thickness of about several nanometers. Moreover, the binding energy peak of C 1s shifts from 284.79 to 284.86 eV, while that of O 1s shifts from 532.23 to 532.44 eV, resulting from oxidation of TP by $AgNO_3$.

Based on all the results above, it can be reasonably deduced that the core is Ag and the shell is polymerized TP. It should be noted that TPs have been used as excellent reductants and stabilizers to synthesize various noble metal nanoparticles and their complexes.[19−23] However, among most previous studies above, there have been few reports that such TP-based composites with core@shell nanostructures were prepared in such an instant manner. Table S1 provides a detailed comparison, indicating that microwave-assisted green chemistry could create novel well-defined nanostructures even if the reactants were the same. In our case, according to the remarkable differences of dielectric loss factors in Ag, TP,

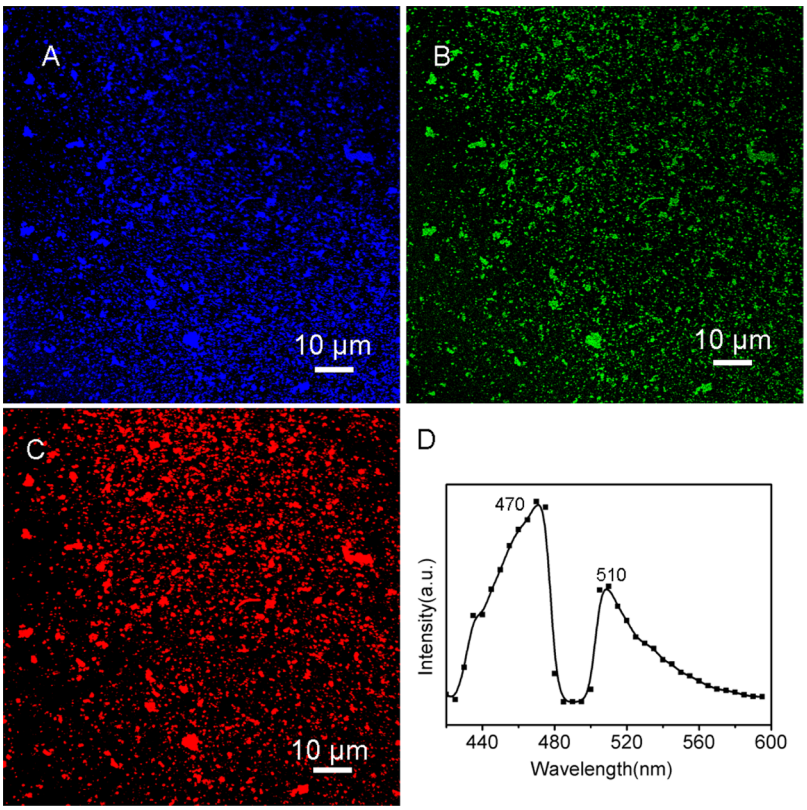

Figure 4. CLSM images of Ag@TP nanoparticles excited at 405 nm and the fluorescence emission image collected in the range of (A) 425−475 nm (blue), (B) 500−550 nm (green), and (C) 600−650 nm (red). (D) Fluorescence emission spectrum from a selected region in the CLSM image of Ag@TP nanoparticles.

and water, it is reasonable to conclude that, under microwave irradiation, fast and selective heating could accelerate redox reaction rates and enhance the phase separation of Ag and TP to quickly form well-defined nanostructures.[24]

To explore the preliminary growth mechanism of Ag@TP nanocomposites, we carried out time-dependent experiments. When $AgNO_3$ aqueous solution was added into the solution of TP, one can see there are many irregular nanoparticles forming, as shown in Figure 5A. In detail, the electronic density of the intermediate is not uniform, indicating that it contains different components. In this case, it could be deduced that they were composed of Ag nanoclusters and partially polymerized TP. After 20 s, they began to aggregate in a special "like-attracts-like" directed way (presented in Figure 5B). This type of aggregation may result from fusion of metal nanoclusters in capping TPs to grow larger mesocrystals, which could be observed in many biomineralization processes.[11] After 50 s, through further aggregation, they became uniform core@shell structures, although uncompleted assembly also appears in the nanostructures (shown as red lines in Figure 5C). It should be noted that when the amont of $AgNO_3$ is much more than that of TP, we could not obtain core@shell nanocomposites but obtained irregular Ag nanoparticles, as revealed in Figure S4. According to the results above, it can be known that, in a single Ag@TP nanoparticle, TPs were cross-linked through oxidation by $AgNO_3$ and self-assembled into the shell surrounding the core of the Ag nanoparticle. However, when adding more $AgNO_3$, polymerized TP could be oxidized further and disassembled into soluble small molecules. As a result, the shell would be removed.

At present, a series of autofluorescent nano/microstructures derived from biomass as units have been developed for various biomedical applications.[25,26] In this study, it is interesting to find that Ag@TP nanoparticles are autofluorescent. Confocal laser scann ing microscopy (CLSM) was employed to examine their multiwave autofluorescent feature. As shown in Figure 4A−C, one can see that the nanoparticles, when excited with a 405 nm laser, exhibit autofluorescence in three typical emission bands: 425−475 nm (blue), 500−550 nm (green), and 600−650 nm (red). Correspondingly, the fluorescence emission spectrum of the selected nanoparticles (Figure 4D) exhibits two peaks at around 470 and 510 nm, in good agreement with the previous report.[18] In this case, it could be considered that the nanoparticles' autofluorescent properties originate from the shell (oxidized TP) rather than the core (Ag nanoparticles), based on the fact that most noble metal nanoparticles were not fluorescent and good quenchers to fluorescent molecules modified on their surfaces.[27−29] A thick enough TP shell (about 10 nm) to some degree still could remain fluorescent because of a

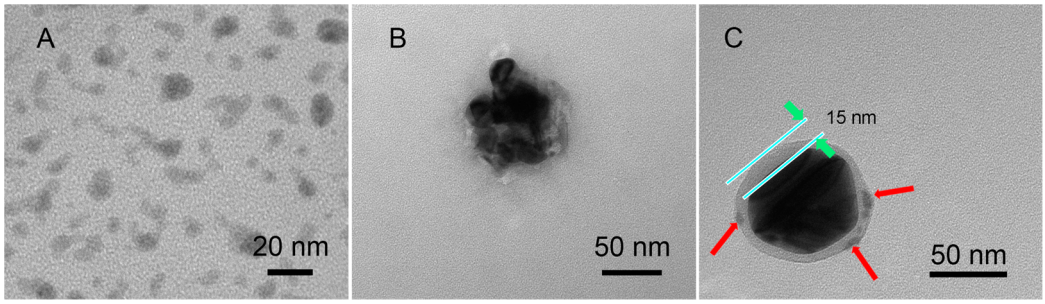

Figure 5. TEM images of Ag@TP nanocomposites collected at different times during the preparation process: (A) 0 s, (B) 20 s, and (C) 50 s.

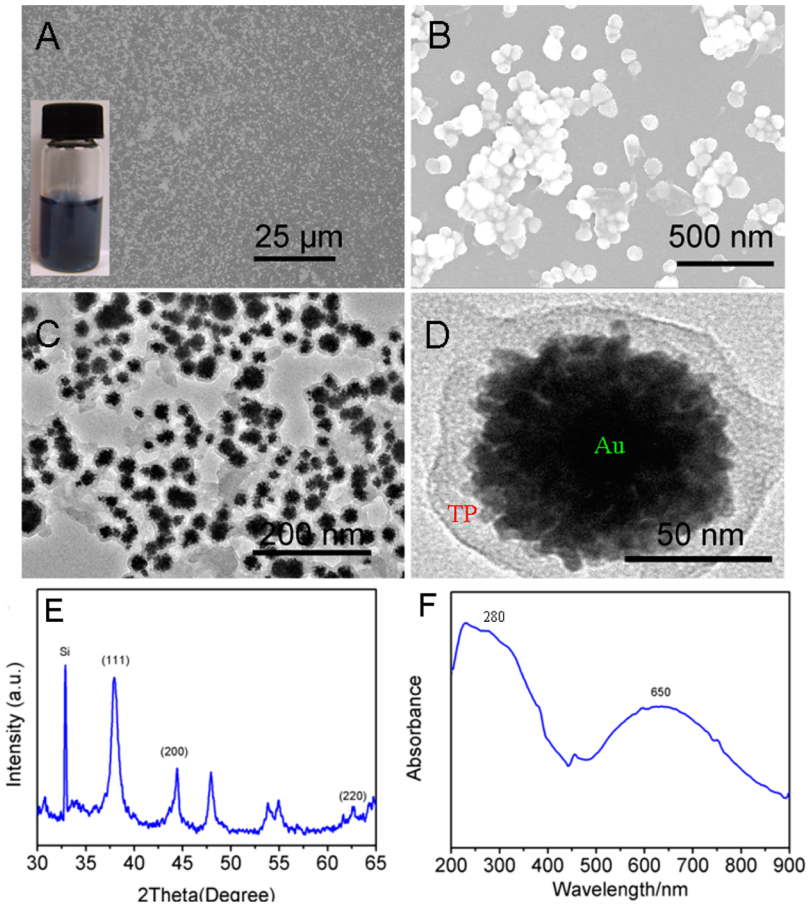

Figure 6. SEM images of Au@TP nanocomposites with (A) lower and (B) higher magnification; TEM images of them with (C) lower and (D) higher magnification; their (E) XRD pattern and (F) UV−vis spectrum dispersed in water. The inset in A is an optical image of Au@TP.

sufficiently high distance between fluorophore and quenching metal nanoparticle. The autofluorescent nanoparticles as-obtained could be developed as a potential biological tracer in biomedical applications, taking notable advantages over traditional fluorochrome-labeled carriers.

This strategy can be extended to other single metal@TP nanosystems. Figure 6A shows that large-scale Au@TP nanoparticles can be prepared. Moreover, Figure 6B shows that the diameter of the nanoparticles is about 100 nm and the surface is rough. A TEM image with lower magnification (Figure 6C) reveals that Au with higher electronic density was around TP with lower electronic density. Figure 6D shows that the inner Au core was composed of smaller Au nanoparticles. Based on the fact that the melting point of Au (1064 °C) is higher than that of Ag (960 °C) under standard conditions, the reason might be proposed that, compared with Ag nanoparticles, it needs more energy and time for smaller Au nanoparticles to aggregate into bigger ones. In addition, as shown in Figure 6E, F, we used XRD and UV−vis spectroscopy to determine the characteristics of Au@TP nanocomposites. The three diffraction peaks shown in Figure 6E correspond to the (111), (200), and (220) diffraction peaks of metallic gold,

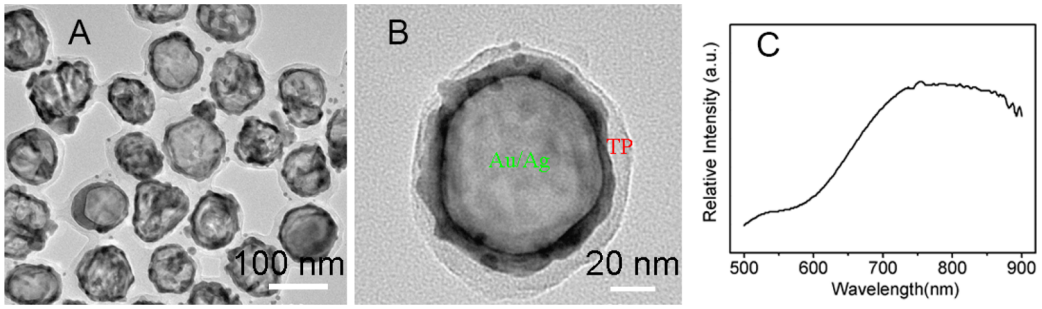

Figure 7. TEM images of hollow Au/Ag@TP nanocomposites with (A) lower and (B) higher magnification. (C) UV−vis−NIR spectrum of Au/Ag@TP nanocomposites.

indicating that the products are composed of crystalline gold. Figure 6F shows Au@TP with interesting optical properties. In detail, the plasmon peak of the product was at about 650 nm which has an approximate 130 nm red shift, compared with that of monodispersed Au nanoparticles synthesized by sodium citrate (shown in Figure S5). It results from aggregation of nanoparticles. Also, there is another absorption peak appearing at 280 nm, similar to that in the case of Ag@TP, revealing coexistence of oxidized TP. Moreover, the relevant EDS pattern in Figure S1B shows that the hybrid nanoparticles were composed of Au and TP.

Considering differences in redox potentials of different noble metal salts in water (Table S2), it can be imagined that more complex multiple metals@TP nanocomposites can be obtained under proper reaction conditions. For instance, after a facile galvanic replacement reaction, hollow Au/Ag@TP bioconjugates were constructed successfully. Figure S1C gives a molar ratio of Au and Ag (about 1:2) in this metal/metal@TP as-prepared, indicating that, during the chemical reaction, Au replaced Ag gradually in Ag@TP without obvious damage of the TP shell. Additionally, Figure 7A,B shows that the Au/Ag@TP was hollow with a diameter similar to that of Ag@TP, which means that the former evolved from the latter. Moreover, Au/Ag@TP as-synthesized with a near-infrared (NIR) absorption at about 800 nm (shown in Figure 7C) could be used for NIR cancer theranostics.[29] Based on the fact that when Pt^{2+} and Pd^{2+} can be reduced by Ag into Pt and Pd, respectively (see Table S2), we believe that, by a similar approach, Pt/Ag@TP and Pd/Ag@TP with similar hollow nanostructures also could be obtained. Furthermore, by proper combination of the strategy, more kinds of alloy@TP could be synthesized.

In general, ideal antibacterial materials should kill harmful micro-organisms with high efficiency without damaging normal cells, tissues, and organs. Due to their antimicrobial activity, silver nanoparticles have become one of the most widely used nanomaterials.[30−32] Recently, Jiang and co-workers reported that silver nanoparticles could inhibit RNA transcription through RNA polymerase−silver binding in erythroid progenitor cells.[33] It can be expected that proper surface modifications of Ag

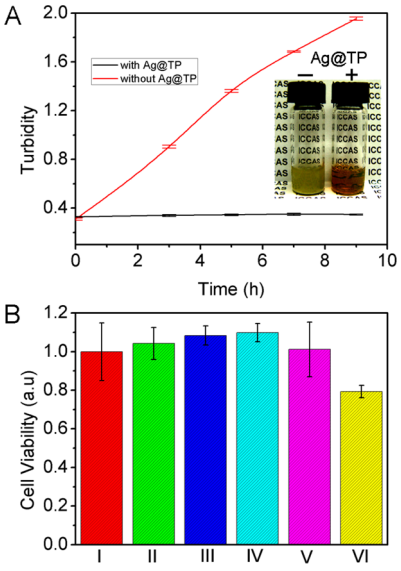

Figure 8. (A) Time-dependent turbidity at 600 nm in E. coli cocultured with and without Ag@TP nanocomposites. The inset is the photo image of E. coli with (right, +) and without (left, −) 0.1 nM Ag@TP nanocomposites after 9 h coculture. (B) COS-7 cell viability, *in vitro*, measured by using the MTT assay (n = 3) in different culture conditions. (I) Without Ag@TP nanoparticles; in the presence of Ag@TP nanoparticles with different concentrations: (II) 0.025; (III) 0.05; (IV) 0.1; (V) 0.2; (VI) 0.4 nM.

nanoparticles could reduce the potential side effects. Herein, as a typical application of Ag@TP nanocomposites, we tried to use them for antibacterial treatment. Through inductively coupled plasma mass spectrometry (ICP-MS) analysis (see Supporting Information), the concentration of Ag@TP can be clarified to fulfill the following quantitative experimental requirements. From Figure 8A, in the control group, one can see that there was a remarkable increase of turbidity in 9 h, indicative of *Escherichia coli* growth. Meanwhile, compared to the control group, there was no change in turbidity when introducing Ag@TP nanocomposites into the culture system. From the inset photo image in Figure 8A, obviously, one can see that there was much more *E. coli* in the control group than in the group cocultured with our product. All of the results above demonstrate that the as-assembled core@shell nanocomposites can function as excellent antibacterial materials. Meanwhile, as shown in Figure 8B, it is very

interesting to find out that Ag@TP at the same or even higher concentrations exhibits no obvious toxicity for normal cells (COS-7) until the concentration of Ag@TP was up to 0.4 nM. Under this condition, about 78% of the cells could survive. It can be speculated that, in this heterogeneous nanostructure, polymerized TP as the shell inhibits the release of Ag^+ from Ag nanoparticles to protect the cells while oxidized TP and leaked Ag^+ can kill the bacteria since TPs are also good antibacterial materials.[34−36] Taken together, the results above indicate that Ag@TP nanoparticles have a great potential for selective antibacterial treatment with no damage to normal tissues or organs.

CONCLUSIONS

In summary, we demonstrate that large-scale autofluorescent polyphenol-based core@shell nanocomposites can be assembled by one-pot preparation under microwave irradiation within 1 min. Time-dependent experiments show that the formation mechanism of core−shell nanocomposites involves with microwave-assisted oxidation-inducing self-assembly and directed aggregation. The strategy above is general to construct single metal@TP nanocomposites. Moreover, we also use a simple galvanic replacement reaction to synthesize hollow Au/Ag@TP bioconjugates with NIR absorption. The results indicate that more complex alloy@TP nanocomposites can be obtained under proper combined reaction conditions. Furthermore, as a typical application of polyphenol-based core@shell heterogeneous nanocomposites, Ag@TP can strongly inhibit *E. coli* growth while they show no obvious toxicity for normal cells, indicating they have great potential as selective antibacterial nanomaterials for biomedical applications in the future.

METHODS

Materials. Tea leaves (broadleaf holly leaf) from Guangdong Province, China, were used as the source of TP. Ethanol, HNO_3, HCl, $AgNO_3$, and $HAuCl_4 \cdot 4H_2O$ were obtained from Beijing Chemical Co. Phosphate buffer saline (PBS) was purchased from Sigma-Aldrich, America. All of chemical reactants are of analytical purity. The microwave oven (G8023CTL-K3) was from Galanz Co., China. The water with an electronic resistance of 18.2 MΩ·cm used was provided by an ELGA Labwater, United Kingdom of Great Britain and Northern Ireland.

Assembly of Metal@TP Nanocomposites. In a typical experiment, 3 g of tea leaves was added to 80 mL of distilled water at 95 °C. After separation from solid that remained after centrifugation (10 000 rpm for 10 min), the tea extract was cooled to room temperature. Then, 2 mL of 4 mM $AgNO_3$ was dropped into 80 mL of the extract at room temperature. Under microwave irradiation at a power intensity of 700 W, the reaction of the mixture was carried out for different times. Finally, the product was obtained by centrifugal separation (10 000 rpm for 10 min) and washed with water and ethanol several times. The preparation procedures of Au@TP nanostructures were the same as that of Ag@TP nanostructures, except replacing 4 mM $AgNO_3$ with 1 mM $HAuCl_4$. Au−Ag@TP nanostructures were obtained through a galvanic replacement reaction by oxidizing Ag@TP nanostructures using 1 mM $HAuCl_4$ at 120 °C in an oil bath.

Characterization. A SEM (Hitachi S-4800, Japan) was used to investigate the morphologies of the products. For TEM observation, the samples were redispersed in ethanol by ultrasonic treatment (SB5200DTD, China) and dropped on carbon−copper grids. TEM images were collected by using a JEM 2010F and 2100F microscope (JEOL, Japan) working at 200 kV. XRD measurements were carried out with a Rigaku D/max-2500 instrument using filtered Cu Kα radiation. CLSM (Olympus FV1000, Japan) was used to check the autofluorescence of Ag@TP nanoparticles. The relevant ICP-MS analysis of Ag@TP nanoparticles was conducted as follows. Ten microliters of Ag@TP nanoparticle aqueous solution was completely digested by 20 mL of aqua regia in a beaker with a volume of 50 mL at mild boiling temperature. The solution was evaporated to 2−3 mL and cooled at room temperature. Subsequently, the sample was diluted by 5% HNO_3 in a 50 mL volumetric flask. Quantification was obtained by external five-point calibration according to the reference method.[28] Details are shown in Supporting Information. FTIR spectra were measured on a Bruker Tensor 27 spectrophotometer using KBr pressed disks. XPS was performed on the Thermo Scientific ESCALab 250Xi using 200 W monochromated Al Kα radiation. The 500 μm X-ray spot was used for XPS analysis. The base pressure in the analysis chamber was about 3×10^{-10} mbar. Typically, the hydrocarbon C 1s line at 284.8 eV from adventitious carbon is used for energy referencing. A U-3010 spectrophotometer (Hitachi, Japan) was used to record the UV−vis spectra of various samples.

Antibacterial Treatment. A single colony of *E. coli* on a solid Luria−Bertani (LB) agar plate was transferred to 5 mL of liquid LB culture medium in the presence of 50 μg mL^{-1} ampicillin and was grown at 37 °C for 12 h. Bacteria were harvested by centrifuging (4000 rpm for 8 min) at 20 °C and washing with PBS three times. The supernatant was removed, and the remaining *E. coli* were resuspended in 20 mL of liquid LB culture medium with or without 0.1 nM Ag@TP nanoparticles in the presence of 50 μg mL^{-1} ampicillin and was grown at 37 °C for 3, 5, 7, and 9 h. Time-dependent turbidity at 600 nm was recorded with a Hitachi U-3010 spectrophotometer when *E. coli* was cocultured with or without 0.1 nM Ag@TP nanocomposites at 37 °C. Data are shown as (mean ± the standard error) from four independent experiments conducted in quadruplicate.

Cell Cultivation. COS-7 cells (monkey fibroblast-like cell line) were cultured in Dulbecco's modified Eagle's medium (DMEM) and 10% fetal bovine serum (FBS) supplemented with 1% penicillin and streptomycin at 37 °C in 5% CO_2, 70% humidity environment, and reseeded every 3 days to maintain subconfluence. When COS-7 cells reached about 90% confluence, they were split into 96-well plates using a standard trypsin-based technique with the final cell concentration of about 2×10^4 cell mL^{-1}. COS-7 cells were incubated in the culture media at a concentration to allow 90% confluence. Free or Ag@TP nanoparticles with different concentrations of 0.025, 0.05, 0.1, 0.2, and 0.4 nM Ag nanoparticles were coincubated with COS-7 cells in the DMEM-containing antibiotics (1% penicillin and streptomycin) and 10% FBS for 24 h before evaluating cell viability in each group.

MTT Cell Viability Assay. Cellular culture medium was aspirated and replaced with 230 μL of DMEM without serum before MTT assays. Twenty microliters of 5 mg mL^{-1} MTT in PBS was added to each well to make MTT with a final concentration of 0.4 mg mL^{-1} and incubated with the cells at 37 °C for 4 h. After the removal of the remaining MTT by aspiration, the purple formazan crystals were dissolved with dimethyl sulfoxide at 200 μL $well^{-1}$ and detected at 570 nm using a wallac 1420 multilabel counter. MTT reduction in untreated cells was set as 100%, and that of treated cells was calculated as a percentage of that of untreated cells. Data are shown as (mean ± the standard error) from three independent experiments conducted in triplicate.

Conflict of Interest: The authors declare no competing financial interest.

Acknowledgment. We acknowledge the financial support of this research by the National Nature Science Foundation of China (21273250, 21007075, and 21321063) and National Basic Research Program of China (973 program, No. 2013CB932802).

Supporting Information Available: The relevant ICP-MS analysis; EDS, FTIR, and XPS patterns; TEM and photo images; UV–vis spectrum; comparison of the relevant reports; the electrode reactions and relevant standard potentials. This material is available free of charge *via* the Internet at http://pubs.acs.org.

REFERENCES AND NOTES

1. Lee, I.; Joo, J. B.; Yin, Y.; Zaera, F. A Yolk@Shell Nanoarchitecture for Au/TiO_2 Catalysts. *Angew. Chem., Int. Ed.* **2011**, *50*, 10208–10211.
2. Chaudhuri, R. G.; Paria, S. Core/Shell Nanoparticles: Classes, Properties, Synthesis Mechanisms, Characterization, and Applications. *Chem. Rev.* **2012**, *112*, 2373–2433.
3. Cao, Y. W. C.; Jin, R. C.; Mirkin, C. A. Nanoparticles with Raman Spectroscopic Fingerprints for DNA and RNA Detection. *Science* **2002**, *297*, 1536–1540.
4. Guo, Y. B.; Tang, Q. X.; Liu, H. B.; Zhang, Y. J.; Li, Y. L.; Hu, W. P.; Wang, S.; Zhu, D. B. Light-Controlled Organic/Inorganic p-n Junction Nanowires. *J. Am. Chem. Soc.* **2008**, *130*, 9198–9199.
5. Ariga, K.; Ji, Q. M.; Mori, T.; Naito, M.; Yamauchi, Y.; Abe, H.; Hill, J. P. Enzyme Nanoarchitectonics: Organization and Device Application. *Chem. Soc. Rev.* **2013**, *42*, 6322–6345.
6. Li, G. L.; Möhwald, H.; Shchukin, D. G. Precipitation Polymerization for Fabrication of Complex Core–Shell Hybrid Particles and Hollow Structures. *Chem. Soc. Rev.* **2013**, *42*, 3628–3646.
7. Yan, X. H.; Blacklock, J.; Li, J. B.; Möhwald, H. One-Pot Synthesis of Polypeptide–Gold Nanoconjugates for *in Vitro* Gene Transfection. *ACS Nano* **2012**, *6*, 111–117.
8. Cui, Y. Y.; Wang, Y. L.; Liu, R.; Sun, Z. P.; Wei, Y. T.; Zhao, Y. L.; Gao, X. Y. Serial Silver Clusters Biomineralized by One Peptide. *ACS Nano* **2011**, *5*, 8684–8689.
9. Sarikaya, M.; Tamerler, C.; Jen, A. K. Y.; Schulten, K. Molecular Biomimetics: Nanotechnology through Biology. *Nat. Mater.* **2003**, *2*, 577–585.
10. Stürzenbaum, S. R.; Höckner, M.; Panneerselvam, A.; Levitt, J.; Bouillard, J.-S.; Taniguchi, S.; Dailey, L.-A.; Ahmad Khanbeigi, R.; Rosca, E. V.; Thanou, M.; *et al.* Biosynthesis of Luminescent Quantum Dots in an Earthworm. *Nat. Nanotechnol.* **2013**, *8*, 57–60.
11. Lee, S. Y.; Gao, X. Y.; Matsui, H. Biomimetic and Aggregation-Driven Crystallization Route for Room-Temperature Material Synthesis: Growth of β-Ga_2O_3 Nanoparticles on Peptide Assemblies as Nanoreactors. *J. Am. Chem. Soc.* **2007**, *129*, 2954–2958.
12. Ejima, H.; Richardson, J. J.; Liang, K.; Best, J. P.; van Koeverden, M. P.; Such, G. K.; Cui, J. W.; Caruso, F. One-Step Assembly of Coordination Complexes for Versatile Film and Particle Engineering. *Science* **2013**, *341*, 154–157.
13. Brott, L. L.; Naik, R. R.; Pikas, D. J.; Kirkpatrick, S. M.; Tomlin, D. W.; Whitlock, P. W.; Clarson, S. J.; Stone, M. O. Ultrafast Holographic Nanopatterning of Biocatalytically Formed Silica. *Nature* **2001**, *413*, 291–293.
14. Danilewicz, J. C. Review of Reaction Mechanisms of Oxygen and Proposed Intermediate Reduction Products in Wine: Central Role of Iron and Copper. *Am. J. Enol. Vitic.* **2003**, *54*, 73–85.
15. Tanaka, T.; Matsuo, Y.; Kouno, I. Chemistry of Secondary Polyphenols Produced during Processing of Tea and Selected Foods. *Int. J. Mol. Sci.* **2010**, *11*, 14–40.
16. Li, C. M.; Xie, B. J. Evaluation of the Antioxidant and Prooxidant Effects of Tea Catechin Oxy-polymers. *J. Agric. Food Chem.* **2000**, *48*, 6362–6366.
17. Weinreb, O.; Mandel, S.; Amit, T.; Youdim, M. B. Neurological Mechanisms of Green Tea Polyphenols in Alzheimer's and Parkinson's Diseases. *J. Nutr. Biochem.* **2004**, *15*, 506–516.
18. Chen, Z. H.; Wang, C. H.; Chen, J. Z.; Li, X. D. Biocompatible, Functional Spheres Based on Oxidative Coupling Assembly of Green Tea Polyphenols. *J. Am. Chem. Soc.* **2013**, *135*, 4179–4182.
19. Nadagouda, M. N.; Varma, R. S. Green Synthesis of Silver and Palladium Nanoparticles at Room Temperature Using Coffee and Tea Extract. *Green Chem.* **2008**, *10*, 859–962.
20. Moulton, M. C.; Braydich-Stolle, L. K.; Nadagouda, M. N.; Kunzelman, S.; Hussain, S. M.; Varma, R. S. Synthesis, Characterization and Biocompatibility of "Green" Synthesized Silver Nanoparticles Using Tea Polyphenols. *Nanoscale* **2010**, *2*, 763–770.
21. Sun, Q.; Cai, X.; Li, J. W.; Zheng, M.; Chen, Z. L.; Yua, C. P. Green Synthesis of Silver Nanoparticles Using Tea Leaf Extract and Evaluation of Their Stability and Antibacterial Activity. *Colloids Surf., A* **2014**, *444*, 226–231.
22. Loo, Y. Y.; Chieng, B. W.; Nishibuchi, M.; Radu, S. Green Synthesis of Silver Nanoparticles Mediated by *Pulicaria glutinosa* Extract. *Int. J. Nanomed.* **2012**, *7*, 4263–4267.
23. Nune, S. K.; Chanda, N.; Shukla, R.; Katti, K.; Kulkarni, R. R.; Thilakavathi, S.; Mekapothula, S.; Kannan, R.; Katti, K. V. Green Nanotechnology from Tea: Phytochemicals in Tea as Building Blocks for Production of Biocompatible Gold Nanoparticles. *J. Mater. Chem.* **2009**, *19*, 2912–2920.
24. Zhu, Y. J.; Chen, F. Microwave-Assisted Preparation of Inorganic Nanostructures in Liquid Phase. *Chem. Rev.* **2014**, *114*, 6462–6555.
25. Jia, Y.; Fei, J. B.; Cui, Y.; Yang, Y.; Gao, L.; Li, J. B. pH-Responsive Polysaccharide Microcapsules through Covalent Bonding Assembly. *Chem. Commun.* **2011**, *47*, 1175–1177.
26. Gao, L.; Fei, J. B.; Cui, W.; Cui, Y.; Li, J. B. pH- and Redox-Responsive Polysaccharide-Based Microcapsules with Autofluorescence for Biomedical Applications. *Chem.—Eur. J.* **2012**, *18*, 3185–3192.
27. Pons, T.; Medintz, I. L.; Sapsford, K. E.; Higashiya, S.; Grimes, A. F.; English, D. S.; Mattoussi, H. On the Quenching of Semiconductor Quantum Dot Photoluminescence by Proximal Gold Nanoparticles. *Nano Lett.* **2007**, *7*, 3157–3164.
28. Dubertret, B.; Calame, M.; Libchaber, A. J. Single-Mismatch Detection Using Gold-Quenched Fluorescent Oligonucleotides. *Nat. Biotechnol.* **2001**, *19*, 365–370.
29. Gao, L.; Fei, J. B.; Zhao, J.; Li, H.; Cui, Y.; Li, J. B. Hypocrellin-Loaded Gold Nanocages with High Two-Photon Efficiency for Photothermal/Photodynamic Cancer Therapy *in Vitro*. *ACS Nano* **2012**, *6*, 8030–8040.
30. Sintubin, L.; Verstraete, W.; Boon, N. Biologically Produced Nanosilver: Current State and Future Perspectives. *Biotechnol. Bioeng.* **2012**, *109*, 2422–2436.
31. Morones, J. R.; Elechiguerra, J. L.; Camacho, A.; Holt, K.; Kouri, J. B.; Ramirez, J. T.; Yacaman, M. J. The Bactericidal Effect of Silver Nanoparticles. *Nanotechnology* **2005**, *16*, 2346–2353.
32. Shahverdi, A. R.; Fakhimi, A.; Shahverdi, H. R.; Minaian, S. Synthesis and Effect of Silver Nanoparticles on the Antibacterial Activity of Different Antibiotics against *Staphylococcus aureus* and *Escherichia coli*. *Nanomedicine* **2007**, *3*, 168–171.
33. Wang, Z.; Liu, S. J.; Ma, J.; Qu, G. B.; Wang, X. Y.; Yu, S. J.; He, J. Y.; Liu, J. F.; Xia, T.; Jiang, G. B. Silver Nanoparticles Induced RNA Polymerase–Silver Binding and RNA Transcription Inhibition in Erythroid Progenitor Cells. *ACS Nano* **2013**, *7*, 4171–4186.
34. Cho, Y. S.; Schiller, N. L.; Oh, K. H. Antibacterial Effects of Green Tea Polyphenols on Clinical Isolates of Methicillin-Resistant *Staphylococcus aureus*. *Curr. Microbiol.* **2008**, *57*, 542–546.
35. Chan, E. W. C.; Soh, E. Y.; Tie, P. P.; Law, Y. P. Antioxidant and Antibacterial Properties of Green, Black, and Herbal Teas of Camellia Sinensis. *Pharmacogn. Res.* **2011**, *3*, 266–272.
36. Friedman, M. Overview of Antibacterial, Antitoxin, Antiviral, and Antifungal Activities of Tea Flavonoids and Teas. *Mol. Nutr. Food Res.* **2007**, *51*, 116–134.